Series interaction and polarization effects in large-angular-momentum two-electron atoms

Michel Poirier
Commissariat à l'Énergie Atomique, Service ''Photons, Atomes et Molécules,'' Centre d'Études de Saclay, F91191 Gif-sur-Yvette Cedex, France

(Received 26 May 2000; published 18 April 2001)

Doubly excited atoms with an outer large-l electron are expected to exhibit moderate series interaction. However, accidental or systematic degeneracies may lead to strong configuration mixing. To describe such phenomena, the present formalism uses a partial diagonalization of the dielectronic interaction plus a second-order correction based on Coulomb Green's function. It makes it possible to determine the eigenfunction composition, level positions, and autoionization widths. While series interaction turns out to be weak for almost degenerate high members of the $4d_j ng$ series in strontium, a significant configuration mixing is observed on $6p_j nl$ series of barium. A generally fair agreement is observed with $6p_j ng$ experimental data. The $6p_j nh$ levels are accurately predicted, too, and new assignations are reported for some of them; however, the computed linewidths are about twice as small as the measured ones. The method also applies to helium and multiply charged ions, where the relevance of collective quantum numbers is analyzed. Some level positions and widths are detailed.

DOI: 10.1103/PhysRevA.63.052513 PACS number(s): 31.25.Jf, 32.80.Dz, 31.15.Md

I. INTRODUCTION

Electronic correlation analyses in doubly excited atoms have given rise to a large amount of literature, both theoretically owing to the development of multichannel quantum defect theory (MQDT) and R-matrix theory [1] or to methods more specifically adapted to helium [2], and experimentally since the advent of tunable laser spectroscopy [3]. In parallel, large-angular-momentum doubly excited states have attracted noticeable interest in the past few years, because of both their stability properties versus autoionization and their ability to be accurately described by *ab initio* treatment. Furthermore, large-l excited states play a prominent role in several domains of physics, such as collisions involving multiply charged ions [4], or recombination processes in plasma physics [5]. When the outer large-l electron wave function hardly overlaps the core-electron wave functions, one may assume that the core-outer-electron interaction is weak and can be described by the first term of the multipolar expansion. Furthermore, the traditional nondegenerate Rayleigh-Schrödinger perturbation theory should apply. This method has been widely used in the past, at first [6–8] and second [9–11] order. However, even large-l series may strongly interact, as some of their terms come accidentally very close; an instance of such a situation is provided by the $6p_{1/2}9g$ and $6p_{3/2}6g$ interaction in barium [12]. Up to now, the connection of such situations to perturbative approaches had not been explored. Therefore, in order to deal properly with such interactions, we propose here a two-step method. First, the electron interaction is diagonalized in a subspace including all the strongly coupled states, i.e., those that are almost degenerated; the composition of the eigenstates gives the configuration mixing. Second, this wave function is corrected by the interaction with nonresonant levels using the traditional second-order perturbation theory. Such a computation can be performed exactly—at least concerning the expansion over the outer electron spectrum—using Coulomb Green's function formalism. We wish to demonstrate here that accurate predictions concerning the atomic level mixing, level positions, and autoionization widths may be achieved when such interactions occur.

The present paper is organized as follows. We develop the basic formalism in Sec. II. Application to the weakly interacting series in alkaline earth atoms are given in Sec. III, namely, for calcium, where the relevance of jk coupling is tested, and for strontium, where we discuss an example of almost perfect zero-order degeneracy. Since a larger amount of data is then available, Sec. IV is devoted to barium, where the $6p_j nl$ series interaction is analyzed and compared to experiment. Section V concerns helium or multiply charged ions for which a series of theoretical approaches exists in the literature. Possible extensions of the method are reviewed in the conclusion.

II. THEORETICAL FRAMEWORK

Let us consider an atom or ion with two active electrons. The inner one is referred to as hereafter the valence electron and let r_2 is its radial coordinate; the outer one is called here the Rydberg electron with coordinate r_1. The other electrons, if any, are called core electrons and are assumed to form an unexcited closed shell. We consider states for which the Rydberg electron has a large angular momentum l so that r_1 is on average greater than r_2 and $1/r_{12}$ is at lowest order approximated by $1/r_1$. The basis of the present treatment is the so-called Heisenberg approximation, where the screened interaction

$$V=\frac{1}{r_{12}}-\frac{1}{r_1} \tag{2.1}$$

is considered perturbatively. Such an approach has been used by a series of authors. For example, in barium Gallagher *et al.* [9] considered the singly excited $6snl$ states with $4\leqslant l\leqslant 7$, while Pruvost *et al.* [10] analyzed the doubly excited $6d_j nl$ states with $6\leqslant l\leqslant 12$. However this decomposi-

tion, often called ''dipolar expansion'' because of the leading term in Eq. (2.1), is not restricted to large-l states since it has also been applied to a wide variety of correlated states in helium [13]. A second-order expansion, not very different from the present formalism, has also been used in molecular physics to obtain the dipole polarizabilities of high-L Rydberg states of H_2 and D_2 through analysis of microwave data [14]. Though this is not explicitly written in Eq. (2.1), the interaction of the outer electron with the core electrons adds up to this V interaction, as discussed previously [8].

If one subtracts the interaction (2.1) from the total Hamiltonian, one gets a zero-order Hamiltonian which separates into the 1 and 2 coordinates, and the Rydberg electron is simply described by a hydrogenic Hamiltonian with a nuclear ''screened'' charge ζ (the net charge of the core is $\zeta+1$, i.e., 2 for helium or alkaline-earth atoms, but isoelectronic ions with $\zeta>1$ may be considered, too). Accordingly, the valence electron behaves as an alkali-atom optical electron and we use here a semiempirical method to derive its radial matrix elements [15]. Exchange effects have been analyzed previously and shown to be moderate for l larger than 3 [16]. We then expect the jk coupling to be the relevant one, and this assumption will receive theoretical support in the next section. From now on, we only need to assume that the spin-orbit effects on the *outer* electron is negligible, while the valence electron spin-orbit effect may compare to the dielectronic interaction.

As an example, the $6p_{1/2}9g$ levels of barium, according to the Heisenberg decomposition, have a zero-order energy equal to the sum of the $6p_{1/2}$ threshold energy and of the Rydberg-electron energy

$$E_1^{(0)}=E_{6p_{1/2}}-R/9^2=60\,941.688\ \ \mathrm{cm}^{-1}, \tag{2.2}$$

where R is the barium Rydberg constant and energies are relative to the neutral-species ground state. The quadrupolar part of the interaction V couples this level to a series of levels, among which is the $6p_{3/2}6g$ with zero-order energy

$$E_2^{(0)}=E_{6p_{3/2}}-R/6^2=60\,939.077\ \ \mathrm{cm}^{-1}. \tag{2.3}$$

It appears that the quadrupolar matrix elements of V are then significantly greater than this separation. For instance, if k is 7/2, one gets

$$\langle 6p_{1/2}9g[k=7/2]|V|6p_{3/2}6g[k=7/2]\rangle=26.7\ \ \mathrm{cm}^{-1}. \tag{2.4}$$

The nondiagonal V element (2.4) is greater than the zero-order energy difference (2.2), (2.3), which precludes the use of ordinary nondegenerate perturbation theory. Therefore, one has to perform a diagonalization of the interaction V in the space spanned by the quasidegenerated states. Zero-order states such as $6p_{3/2}6g$ will be called ''configurations'' in the following. The matrix elements of V in the subspace $n_il_ij_in_el_e[k]$ are easily computed in the jk scheme with the long-range approximation (equivalent to neglecting exchange) [16]. The diagonalization involves matrices of small dimensions for which a standard Jacobi procedure [17] turned out to be completely satisfactory.

Once we have obtained the eigenstates and the eigenvalues of the interaction V, we may compute accurate energy levels correcting these eigenvalues through traditional second-order perturbation theory. This additional step is required because it has been emphasized [11] that second-order dipole-dipole interaction is of the same order of magnitude as the quadrupolar interaction dealt with in the diagonalization process. The only difference with the previous second-order formalism is the following: in the infinite sum one has to omit all the states that span the diagonalization subspace. Namely, if $\mathcal{E}$ is such subspace, the diagonalization procedure results in the determination of the eigenstates

$$|\alpha\rangle=\sum_{i\in\mathcal{E}}\langle i|\alpha\rangle|i\rangle, \tag{2.5}$$

where i denotes the basis elements of this subspace, or ''configurations.'' The second-order correction to the energy of this eigenstate is then given by

$$\Delta^{(2)}(\alpha)=\sum_{i\in\mathcal{E},\ i'\in\mathcal{E}}\langle i|\alpha\rangle\langle\alpha|i'\rangle\sum_{j\notin\mathcal{E}}\frac{\langle i'|V|j\rangle\langle j|V|i\rangle}{E_\alpha-E_j}. \tag{2.6}$$

In this equation, the E_α energy in the denominator can simply be chosen as the zero-order energy of the i state closest to eigenstate α (i.e., with maximum projection) or as the α eigenenergy as derived from diagonalization. Since such a denominator is nonresonant, both values give approximately the same level shift. While the projection coefficients $\langle i|\alpha\rangle$ are obtained from the diagonalization procedure, the infinite sum over j is deduced from a method already sketched [11]. One has to take care that j configurations in $\mathcal{E}$ are to be subtracted from the sum, which thus involves ''reduced'' Green's functions instead of ordinary ones.

Finally one may notice that if at least one of the states i involved in the diagonalization may autoionize, the denominator in sum (2.6) may vanish for j states in the continuum; one then adds a small positive imaginary part to the denominator and the second-order element $\Delta^{(2)}$ is now complex:

$$\Delta^{(2)}=\delta E^{(2)}-i\Gamma/2, \tag{2.7}$$

$\delta E^{(2)}$ being, as above, the second-order shift and Γ the autoionization width of the eigenstate, computed at first order, i.e., through the Fermi Golden Rule, but accounting for configuration mixing.

Computational details are as follows. The matrix elements of the V operator are obtained for the valence electron part using a semiempirical model [15] where the input data are the parent-ion energy spectrum and the grandparent (closed-shell core) polarizabilities and core size. The parent-ion energies are taken from measurements, while we use the dipolar and quadrupolar polarizabilities available in the literature [18]. The Rydberg electron bound-bound matrix elements of V are deduced from recursion relations quite similar to the one obtained in the bound-free case [19]; concerning the ''on-shell'' elements, i.e., $\langle n_il_i|r^{-t-1}|n_j=n_il_j\rangle$, one may even use closed analytical expressions such as those derived from group theory [20].

TABLE I. Eigenfunction composition of the $3d_j5l[k=7/2]$ levels in calcium. The traditional composition percentages are the square of the tabulated coefficients.

Eigenfunction	$3d_{3/2}5d$	$3d_{3/2}5g$	$3d_{5/2}5d$	$3d_{5/2}5g$
$\alpha=1$	0.9074	-5.0×10^{-3}	-0.4202	-9.4×10^{-3}
$\alpha=2$	9.7×10^{-3}	0.9927	6.4×10^{-3}	-0.1204
$\alpha=3$	0.4202	-1.08×10^{-2}	0.9073	-7.4×10^{-3}
$\alpha=4$	-4.3×10^{-3}	0.1204	1.15×10^{-2}	0.9927

The second-order correction involves an infinite sum over the principal quantum numbers of the inner and outer electrons. As detailed previously [21], on the one hand the inner-electron sum is replaced by a numerical truncated sum; this approximation relies on the rapid decrease of such elements when the principal quantum number of the alkalilike ion increases [15,22]. On the other hand, the outer-electron sum is performed exactly using the Coulomb Green function, for which the Sturmian representation often provides an efficient method of computation [23].

As in the nondegenerate case [21], the core polarization shifts these energy levels. The effect on the inner electron is automatically accounted for because the zero-order energy levels are taken from experiment and thus include this polarization. In a previous paper [8] we established that the core polarization by *both* active electrons is implicitly considered provided the inner-electron matrix elements are properly screened. Finally, the outer-electron contribution to core polarization is obtained by evaluating the matrix elements of

$$V_{\mathrm{pol}}=-\tfrac{1}{2}\alpha_{\mathrm{d}}r_1^{-4}-\tfrac{1}{2}\alpha_{\mathrm{q}}r_1^{-6}. \tag{2.8}$$

The mean value of this operator for the eigenstate α is given by

$$\Delta_{\mathrm{pol}}=\sum_{\substack{i\in\mathcal{E}\\ j\in\mathcal{E}}}{}'\langle i|\alpha\rangle\langle\alpha|j\rangle\langle n_jl_i|V_{\mathrm{pol}}|n_il_i\rangle, \tag{2.9}$$

where the prime in the sum means that it is restricted to configuration pairs $i=\{n_{vi}l_{vi}j_{vi}n_il_i\}$, $j=\{n_{vj}l_{vj}j_{vj}n_jl_j\}$ such as $n_{vi}=n_{vj}$, $l_{vi}=l_{vj}$, $j_{vi}=j_{vj}$, and $l_i=l_j$, i.e., with all quantum numbers identical except possibly the outer-electron principal quantum numbers.

III. SERIES INTERACTION IN CALCIUM AND STRONTIUM

In calcium and strontium, moderate series interactions can be analyzed within the present formalism. A rather large amount of experimental data is available for comparison.

A. Calcium

The $3d_jng[k]^e$ states of calcium have been investigated in detail [24–26]. We first consider the $n=5$ levels for which the electrostatic coupling is greatest compared to the $3d_{3/2}-3d_{5/2}$ fine-structure splitting (the electronic interaction is expected to decrease as n^{-3}). In order to compare the $1/r_{12}$ matrix elements with this splitting, we analyze the $3d_{3/2}nl[k]$ and $3d_{5/2}n'l'[k]$ couplings with $n'=n$ and l,l' compatible with the given angular momentum and parity. For instance, for $k=7/2$ and parity even, the configurations involved in the diagonalization are $3d_{3/2}5d,3d_{3/2}5g$, $3d_{5/2}5d,3d_{5/2}5g$. The diagonalization in this 4×4 subspace gives the eigenstates as detailed in Table I. It appears that the configurations with different outer l are almost not mixed. This is satisfactory for several reasons. First, the $3d_jnd$ states are certainly not well described here because the inner and outer wave functions significantly overlap. But the present analysis points out that the $3d_jng$ states behave mostly independently of them and therefore the results for the g states are certainly reliable. Second, it is an indication that a more complex problem, where the diagonalization would involve much more configurations, may reasonably be split into several parts, the diagonalization within the (even smaller) subspace with given outer l being almost sufficient.

In view of the Table I results, we can assign the relevance for the jk or Lk coupling scheme. One can check that jk coupling holds very well for $3d5g$ states in calcium. For example if for each k one denotes through α_1 the eigenstate that is closest to the jk-coupled $|3d_{3/2}5g[k]\rangle$ one gets

$$\langle 3d_{3/2}5g|\alpha_1\rangle=0.9798 \quad \text{if } k=5/2, \tag{3.1}$$

$$=0.9927 \quad \text{if } k=7/2, \tag{3.2}$$

$$=0.9999 \quad \text{if } k=9/2, \tag{3.3}$$

$$=0.9737 \quad \text{if } k=11/2. \tag{3.4}$$

The square of these quantities, giving the traditional percentage of configuration $3d_{3/2}5g[k]$ in the considered eigenstates, ranges from 94% to almost 100%. This analysis reinforces the statement that jk coupling is relevant for series such as Nd_jng: for instance, in calcium, if $n>5$ the electronic interaction, i.e., the V matrix element, decreases roughly as n^{-3} and therefore the jk coupling is even more relevant higher in the series. Of course this statement does not apply if series interaction is important, as will be illustrated in the barium section. Considering the alkali-earth atoms heavier than calcium, the inner-electron spin-orbit effect increases while the electronic interaction remains approximately the same; therefore, here again jk coupling is fully relevant for states such as $4d_jng$ in strontium and $5d_jng$ in barium.

Alternately, the same analysis proves that the $3d_jnd[k]$ states closely obey Lk coupling—in fact, LS would be even more relevant for low n values but the outer electron spin is

TABLE II. Eigenstates resulting from the interaction of the even $4d_{3/2}23l$ and $4d_{5/2}15l$ energy levels in strontium. The diagonalization is performed for all even-parity levels with $3/2 \leqslant k \leqslant 13/2$; results are displayed only for dominant configuration with an outer g or i electron. The experimental and R-matrix results for $k=3/2$, 5/2 are from Goutis *et al.* Ref. [30]. The $k=7/2$ and 9/2 assignation to experimental data [31] is an interpretation according to the present analysis.

			Position (cm^{-1})			
k	Leading configuration	Other configuration	Present paper	Second order	Experiment	R-matrix
3/2	$4d_{5/2}15g$ (95.7%)	$4d_{3/2}23d$ (3.7%)	60 277.55	60 277.18	60 277.55	60 277.55
5/2	$4d_{3/2}23g$ (68.9%)	$4d_{5/2}15g$ (30.9%)	60 278.78	60 279.45	60 279.5	60 279.8
5/2	$4d_{5/2}15g$ (68.9%)	$4d_{3/2}23g$ (30.9%)	60 278.01	60 277.47	60 277.5	60 277.5
7/2	$4d_{3/2}23g$ (68.4%)	$4d_{5/2}15g$ (31.5%)	60 278.98	60 279.78		
7/2	$4d_{5/2}15g$ (68.9%)	$4d_{3/2}23g$ (31.5%)	60 278.69	60 277.89	60 277.7	
7/2	$4d_{5/2}15i$ (100%)		60 281.71	60 280.71		
9/2	$4d_{3/2}23g$ (98.9%)	$4d_{5/2}15g$ (1.1%)	60 280.07	60 280.12		
9/2	$4d_{5/2}15g$ (98.9%)	$4d_{3/2}23g$ (1.1%)	60 278.57	60 278.45	60 278.4	
9/2	$4d_{3/2}23i$ (67.0%)	$4d_{5/2}15i$ (33.0%)	60 280.51	60 280.61		
9/2	$4d_{5/2}15i$ (67.0%)	$4d_{3/2}23i$ (33.0%)	60 280.59	60 280.49		
11/2	$4d_{3/2}23g$ (90.3%)	$4d_{5/2}15g$ (9.7%)	60 280.40	60 280.42		
11/2	$4d_{5/2}15g$ (90.3%)	$4d_{3/2}23g$ (9.7%)	60 279.14	60 279.16		
11/2	$4d_{3/2}23i$ (71.2%)	$4d_{5/2}15i$ (28.8%)	60 280.51	60 280.54		
11/2	$4d_{5/2}15i$ (71.2%)	$4d_{3/2}23i$ (28.8%)	60 280.35	60 280.32		
13/2	$4d_{5/2}15g$ (100%)		60 280.06	60 280.05		
13/2	$4d_{3/2}23i$ (99.8%)	$4d_{5/2}15i$ (0.2%)	60 280.53	60 280.53		
13/2	$4d_{5/2}15i$ (99.8%)	$4d_{3/2}23i$ (0.2%)	60 280.26	60 280.26		

ignored here. For example if $k=5/2$, the same diagonalization that gave the above quoted α_1 gives, among other eigenvectors,

$$\langle 3d5dF[5/2]|\alpha_F\rangle = 0.9951, \tag{3.5}$$

the subscript F being here merely to convey that this is the eigenstate with maximum projection on $3d5dF[5/2]$.

B. Strontium

As our next example, we now consider the even-parity $4d_jnl$ series in strontium. The data used in our computation are the ion energy levels from Moore [27] with $7p_j$ levels amended according to Lange *et al.* [28], while the ionization potentials are from Esherick [29] for Sr and Lange *et al.* [28] for Sr^+. Large-l doubly excited levels have been investigated by Goutis *et al.* [30] in the $J=1,2$ case and by Jimoyiannis *et al.* [31] in the $J=3,4,5$ case, the former paper containing an R-matrix-based theoretical analysis too. Special attention is paid here to the $4d_{3/2}23l-4d_{5/2}15l'$ interaction. Indeed, using the above-mentioned spectroscopic references, the zero-order energies for these levels are 60 280.65 cm^{-1} and 60 280.71 cm^{-1}, which means almost exact degeneracy. However, it was stated in our previous analyses on positions [21] and widths [32] that usual nondegenerate perturbation theory with only dipole interaction included at second order was adequate. We can justify this attitude as follows. Our results concerning the $4d_jng$ and $4d_jni$ are detailed in Table II. Though all l outer-electron angular momenta values compatible with k between 3/2 and 13/2 were included in the computation, only $4d_jng$ and $4d_jni$ are included in this table: the positions for $l=0$ or 2 would not be reliable within the current formalism, while the l values greater than 7 are far from experimental investigation and almost behave as pure hydrogenic levels. In this table, the second column is the label attributed to the eigenstate according to the present diagonalization; the percentage of the leading configuration is indicated between parentheses. In the third column, we mention the next important configuration and its percentage. The fourth column contains the newly derived position with respect to the ground state of Sr, while the fifth one refers to our second-order computation [21]. The sixth column is from Ref. [30] for $k=3/2,5/2$ and from Ref. [31] for $k=7/2,9/2$, and the last column contains the theoretical predictions appearing in Ref. [30].

A rapid inspection of Table II shows that large-l state mixing is, in some cases, far from negligible. For instance, the eigenstate labeled $4d_{3/2}23g[k=7/2]$ contains almost 32% of $4d_{5/2}15g[k=7/2]$ character, but this results in a <1 cm^{-1} difference in the energy position compared to the ''traditional'' nondegenerate second-order perturbation in the fifth column [21]. It must be mentioned that this nondegenerate perturbation calculation *must* only include the second-order dipolar correction—such as the interaction between $4d_jng$ and $5p_jnh$; if the quadrupolar contribution to these second-order positions had been included, one would have observed an unphysical quasidivergence on the positions, due to the $4d_{3/2}23l-4d_{5/2}15l$ accidental degeneracy.

TABLE III. Position and width of the interacting $6p_{1/2}9g[k]$ and $6p_{3/2}6g[k]$ levels in barium. In each pair of data, the first one is the energy with respect to the ground state of neutral barium, and the second is the autoionization width. All data are in cm^{-1}. The second and third columns are the second-order computation ignoring the quadrupolar coupling between both $6p_j$ series: only dipolar interaction is included at second order. The next three columns detail the results from diagonalization plus second-order correction: the number in parentheses is the percentage of the dominant configuration in the eigenstate. The experimental data are from Ref. [12]. The zero-order energies are 60 941.69 cm^{-1} and 60 939.08 cm^{-1} for the $6p_{1/2}9g$ and $6p_{3/2}6g$ levels, respectively. The $6p_{3/2}6g[11/2]$ is weakly mixed with the $6p_{1/2}9i[11/2]$, which is included in the diagonalization but not tabulated here.

State	Second order		Diagonalization		Experiment	
$6p_{3/2}6g[5/2]$	60 979.83	22.25	(99%) 60 978.68	25.47	60 979.2±3.6	23.76±7.13
$6p_{1/2}9g[7/2]$	60 939.37	8.43	(70%) 60 953.52	15.5		
$6p_{3/2}6g[7/2]$	60 904.37	16.85	(70%) 60 889.37	11.88	60 889.1±2.1	14.03±4.21
$6p_{1/2}9g[9/2]$	60 939.79	10.37	(90%) 60 945.70	13.15	60 943.1±1.1	14.42±2.16
$6p_{3/2}6g[9/2]$	60 878.31	15.86	(90%) 60 872.48	13.16	60 868.5±1.0	13.47±2.02
$6p_{3/2}6g[11/2]$	60 954.84	23.72	(96%) 60 956.56	22.65	60 942.9±1.8	23.32±3.50

Amazingly enough, the second-order results of column 5 seem to be even more accurate than the present data derived from diagonalization; a possible though not definite explanation might lie in some inaccuracy of the $4d_j$ levels in Sr, a fraction of cm^{-1} being significant here. Our main conclusion from this analysis will be that this degeneracy hardly manifests itself in significant levels shifts (below the cm^{-1} here), though state mixing is indeed important. Such a behavior originates in the fact that we are dealing here with high members of Rydberg series with rather different n values, thus the nondiagonal couplings remain moderate.

IV. SERIES INTERACTION IN BARIUM

A situation rather different from the $4d_jnl$ series interaction in strontium will be provided by the barium case where the $6p_{1/2}9l$ and $6p_{3/2}6l$ states—and, to a lesser extent, the $6p_{1/2}14l$ and the $6p_{3/2}7l$ states—interact much more significantly. A series of experimental data is available for $6p_jng$ states [12] and for $6p_jnf,nh$ states [33]. Jones and Gallagher [7] performed an investigation of the l dependence of quantum defects and autoionization widths for the $6p_{1/2}nl$ series with n from 11 to 13 and l from 4 or 5 to $n-2$ or $n-1$, but we do not expect strong series interaction in this n range. Accordingly, Pruvost *et al.* [10] studied the $6p_{3/2}nl$ levels with n from 11 to 15 and l from 5 to $n-1$, but they all lie above the $6p_{1/2}$ threshold and therefore do not interact strongly with discrete members of the $6p_{1/2}nl$ series.

A. $6p_jng$ states

The data from Jaffe *et al.* [12] are a useful test of the present diagonalization procedure. Moreover, since our previous works [11,21,32] concerned the position and width of the lower $5d_jnl$ series, some new theoretical values using plain second-order theory will equally be given here on $6p_jng$ states outside the strong interaction regions.

Our results about interacting members of the $6p_jng$ series are detailed in Tables III and IV. The second-order computation in second and third columns is performed according to our previously detailed formalism [21,32]. For the sake of consistency, at first perturbation order the interaction V is expanded up to the quadrupolar contribution, while at second order it is expanded up to the dipolar term only; these truncations arise from consideration that the dominant contribution to third order, neglected here, should scale as the octopolar contribution at first order or as the dipole-quadrupole contribution at second order (see, e.g., Ref. [11] for a simple argument). One should mention that in the $k=5/2$ and 7/2 results displayed in the present tables, the $6d_jnp[k]$ contri-

TABLE IV. Position and width of the interacting $6p_{1/2}14g[k]$ and $6p_{3/2}7g[k]$ levels in barium. See Table III for details. The zero-order level positions are 61 736.58 and 61 747.80 cm^{-1} for $6p_{1/2}14g$ and $6p_{3/2}7g$, respectively. In addition to the 61 714.8 cm^{-1} level that was labeled $6p_{3/2}7g[7/2]J=3$ in Ref. [12], we propose here to label their unassigned 61 716.6 cm^{-1} level as $6p_{3/2}7g[7/2]J=4$.

State	Second order		Diagonalization		Experiment	
$6p_{3/2}7g[5/2]$	61 772.32	16.80	(100%) 61 772.24	16.86	61 771.1±2.5	16.56±4.97
$6p_{1/2}14g[7/2]$	61 735.84	5.51	(55%) 61 742.61	8.76	61 742.8±0.6	4.03±1.21
$6p_{3/2}7g[7/2]$	61 725.15	12.72	(55%) 61 718.19	6.76	61 714.8±1.6	10.96±3.29
					61 716.6±0.68	9.09±1.36
$6p_{1/2}14g[9/2]$	61 735.95	3.13	(88%) 61 738.23	5.42	61 736.3±0.29	3.83±0.57
$6p_{3/2}7g[9/2]$	61 708.72	12.07	(88%) 61 706.49	9.82	61 703.4±0.77	10.29±1.56
$6p_{3/2}7g[11/2]$	61 756.81	18.27	(99%) 61 756.99	18.15	61 747.0±1.34	17.83±2.67

bution to the second-order shift has been subtracted. These perturbing series both for $j=3/2$ and 5/2 give rise to an unphysical quasiresonance because the $6p_{3/2}6g$ has a zero-order energy $E(6p_{3/2})-R/6^2$ almost equal to $E(6d_j)-R/2^2$ but the $6d_j2p$ falls completely outside the present formalism; large-l techniques obviously do not apply to p electrons, and in barium $2p$ is a filled orbital that cannot be handled like vacant orbitals.

Examination of Table III shows that the current diagonalization plus second-order formalism provides positions and widths in fair agreement with the experimental data, especially for the lowest k states. For instance, in the $k=7/2$ case where the $6p_{1/2}9g-6p_{3/2}6g$ mixing is significant (the eigenstate on the third row has 70% $6p_{3/2}6g$ character and 30% $6p_{1/2}9g$ character), the diagonalization improves significantly the agreement with the experimental position; experimental data about the $6p_{1/2}9g[7/2]$ would be useful since the widths predicted from second-order theory and diagonalization differ by almost a factor of 2. The only indication in Ref. [12] is that, except for $n=14$, the $6p_{1/2}ngJ=3$ (i.e., $[k=7/2]$) feature observed in linear polarization lies $0.002n^{-3}$ above the $[k=9/2]J=5$ feature and is broader, which is in qualitative agreement with the present paper. As a rule, all the widths computed through diagonalization fall inside the experimental error bars; these bars are rather large; however, the $6p_{1/2}9g[9/2]$ is correctly described using diagonalization and not through plain second-perturbation order. Finally, one must state that the largest k values are systematically predicted above the experimental data, as much as 14 cm^{-1} if n equals 6; though the definite explanation for that remains unclear, it might originate in the lack of high-lying perturbers included at second order, which could be more sensitive here than for low k because angular factors differ; another possible reason might lie in the quadrupolar interaction $6p_{3/2}6g[11/2]-6p_{1/2}\nu i[11/2]$ with $\nu\simeq 9$; a simple second-order computation ignoring degeneracy shows that such a quadrupolar interaction shifts the $6p_{3/2}6g[11/2]$ by -16.5 cm^{-1}, but a diagonalization involving, e.g., $6p_{1/2}\nu i$ with $7\leqslant\nu\leqslant 10$ would be useful. The analysis of $6p_{3/2}ng[k=11/2]$ quantum defects detailed below corroborates this assumption. Finally, one must note that here widths are predicted more accurately than positions; this stems from the fact that first-order computation of widths, which is sufficient here, only involves a finite sum on ''perturber'' levels, i.e., the various ionization thresholds; conversely, the computation of shifts must always be performed up to the second order at the minimum, and this involves an infinite sum over the two-electron atomic spectrum, in which truncation is not avoidable.

The inspection of Table IV concerning the $6p_{1/2}14g-6p_{3/2}7g$ interaction leads to similar conclusions. The diagonalization procedure significantly improves the agreement with experiment except for the highest k value. The present analysis allows us to assign the unidentified 61 716.6 cm^{-1} level of Ref. [12] as $6p_{3/2}7g[k=7/2]$ $J=4$; we may attibute the 1.8 cm^{-1} departure from the $[k=7/2]$ $J=3$ position partly to experimental uncertainty and partly to pair splitting, i.e., weak exchange effects.

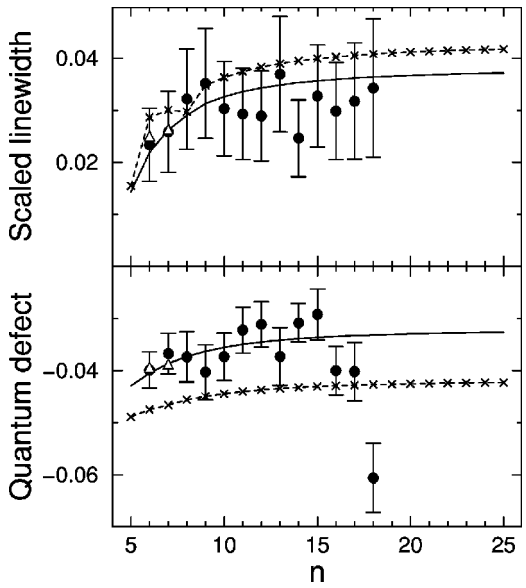

FIG. 1. Quantum defects and scaled autoionization linewidths of the $6p_{3/2}ng[k=5/2]$ states of barium. The scaled linewidth $n^3\Gamma$ is in atomic units. The filled circles are experimental data from Ref. [12]. The solid and broken lines are the present second-order computations, with quadrupoles included at second order for the broken line. The solid line for the width may be accurately fitted to $0.0385-0.603/n^2$ below the $6p_{1/2}$ threshold ($n\leqslant 8$) and to $0.0381-0.543/n^2$ above. For $n=6$ and 7, the open triangles are the partial diagonalization results as displayed in Tables III and IV.

To analyze the quantum defects and scaled linewidths across the whole series, we have plotted in Figs. 1–4 these quantities for the $6p_{3/2}ng[k]$ states with k from 5/2 to 11/2. The theoretical predictions from second-order perturbation including or not including the quadrupolar interaction at second order (i.e., terms such as $\langle 6p_{3/2}ng|r_<^2/r_>^3|6p_{1/2}\nu g\rangle^2/\Delta$, where Δ is an energy denominator) are compared to available experimental data.

In Fig. 1 for $k=5/2$, it appears that, omitting the $n=6$ and 7 cases previously analyzed, the agreement between second-order perturbation theory ignoring the quadrupolar terms and experiment is fine. The inclusion of quadrupoles at second order changes significantly the quantum defects (and to a lesser extent, the scaled linewidths) with usually degraded agreement with experimental data; it involves the interaction of the $6p_{3/2}ng[5/2]$ states with the $6p_{1/2}\nu d[5/2]$ states, which are certainly poorly described within the present large-l formalism. Besides, one can see that the strong variation of the experimental quantum defect for $n>15$, without simultaneous variation of the scaled linewidth, does not relate to the presence of any perturber in this region, as far as we know. This probably indicates an underestimate of certain error bars. Though it would be more apparent on a scaled-width-versus-energy plot, the linewidth computed at second order including dipoles (solid line in the top half of Fig. 1) accurately follows a two-term law with a discontinuity when crossing the threshold. Conversely, the corresponding quantum defects (solid line in the bottom half of Fig. 1) are reasonably fitted with three terms, namely, here $\delta=-0.032-0.38/n^2+2.69/n^4$ whatever the value of n.

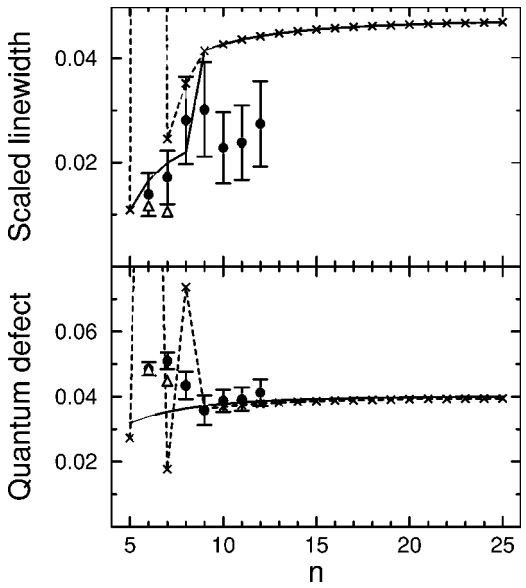

FIG. 2. Quantum defects and scaled autoionization linewidths of the $6p_{3/2}ng[k=7/2]$ states of barium. See Fig. 1 for details. The second-order results including quadrupoles would be ''divergent'' for $n=6$ because of the interaction with $6p_{1/2}9g[7/2]$, and do not appear on the graph. For instance, one would get here a quantum defect of 0.28 and a scaled linewidth of 0.85. Then the diagonalization procedure (triangle) is the only reliable one. The solid line for the width may be fitted to $0.0292-0.456/n^2$ below the $6p_{1/2}$ threshold and to $0.0478-0.508/n^2$ above.

As seen in Fig. 2, the data concerning $6p_{3/2}ng[k=7/2]$ are less abundant. For n greater than 8, the present quantum defects agree fairly well with experiment, and inclusion of quadrupoles at second order has almost no effect either on positions or on widths. Rather intriguing is the disagreement

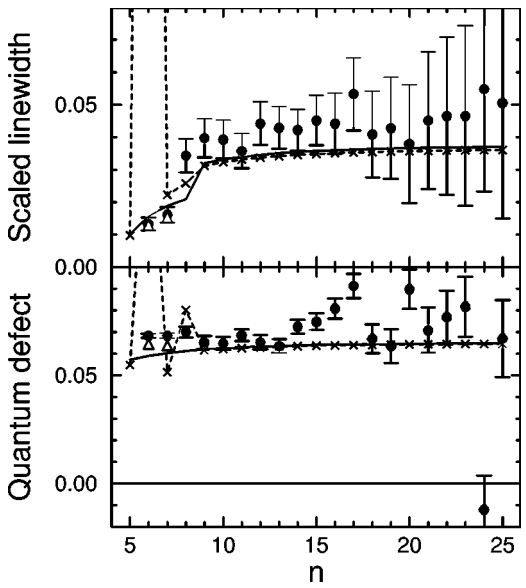

FIG. 3. Quantum defects and scaled autoionization linewidths of the $6p_{3/2}ng[k=9/2]$ states of barium. The solid line for the width may be fitted to $0.0279-0.446/n^2$ below the $6p_{1/2}$ threshold and to $0.0378-0.465/n^2$ above. See Fig. 1 for details.

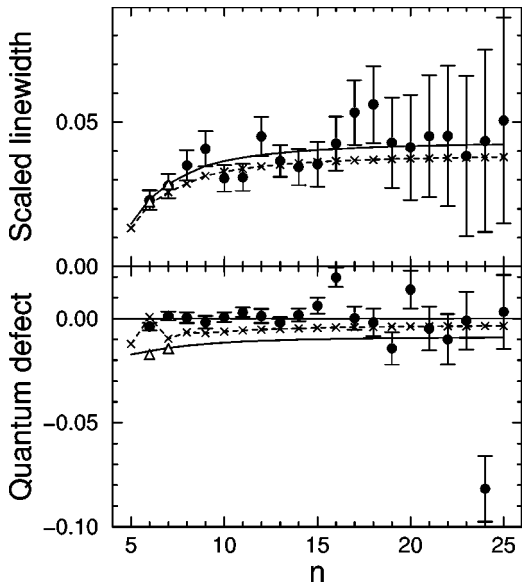

FIG. 4. Quantum defects and scaled autoionization linewidths of the $6p_{3/2}ng[k=11/2]$ states of barium. The solid line for the width may be fitted to $0.0430-0.706/n^2$ below the $6p_{1/2}$ threshold and to $0.0434-0.688/n^2$ above. See Fig. 1 for details.

by a factor of 2 concerning the linewidths in the same region; one might conclude that the fine-structure autoionization process $6p_{3/2}ng \rightarrow 6p_{1/2}\epsilon l$ responsible for the jump in the theoretical width when n changes from 8 to 9 is simply absent from experiment! The fine agreement between both theoretical predictions for $n \geqslant 9$ means that second-order (quadrupole-dipole) corrections to the width such as $6p_{3/2}ng-6p_{1/2}\nu g-5d_{3/2}\epsilon h$ weakly contribute to the total width. Besides, a detailed examination of the partial widths demonstrates that the fine-structure autoionization process is well described by the first-order quadrupolar amplitude, the second-order dipole-dipole amplitude providing here a positive correction of only about 4%. This differs strongly from the $5d_jng$ states of barium [11,34] where the second-order correction was large and with a negative sign. Brief mention should be made of the $6p_{3/2}8g$ state, lying just below the $6p_{1/2}$ threshold; it is close to the $6p_{1/2}68g$ state but the n difference is so large that such coupling is likely to be small. However, the second-order computation including quadrupoles gives a ''divergent'' quantum defect of 0.074, far from the prediction without quadrupoles (0.036); the coupling between $6p_{3/2}8g$ and $6p_{1/2}\nu g$ is here responsible for a -16.3 cm^{-1} shift. A more realistic treatment would involve a diagonalization including all the $6p_{1/2}\nu g$ states lying within the $6p_{3/2}8g$ linewidth. This procedure is probably unnecessary, since the simple second-order computation without quadrupoles is almost in agreement with experiment (twice the error bar).

The $k=9/2$ case displayed in Fig. 3 leads to rather similar conclusions. The agreement in scaled linewidths is satisfactory if we ignore the $n=8$ case for the reason mentioned just above. The rather large error bar for $n=24$ allows an acceptable agreement between our prediction and experiment; the disagreement by a factor of 0.68 had been incorrectly attributed to the absence of second-order autoionization ampli-

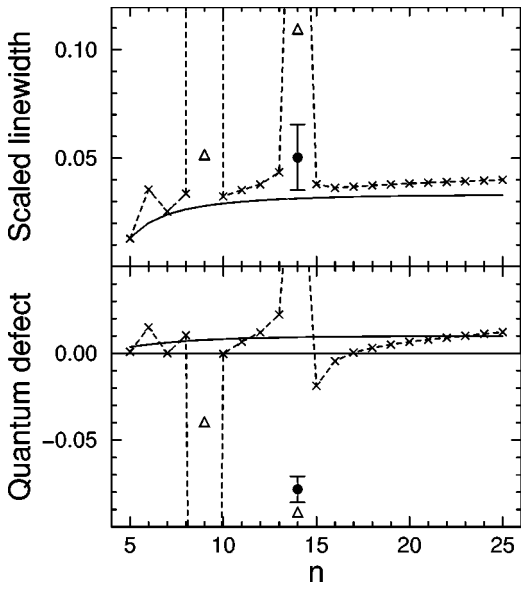

FIG. 5. Quantum defects and scaled autoionization linewidths of the $6p_{1/2}ng[k=7/2]$ states of barium. The solid line for the width may be fitted to $0.0339-0.502/n^2$. See Fig. 1 for details.

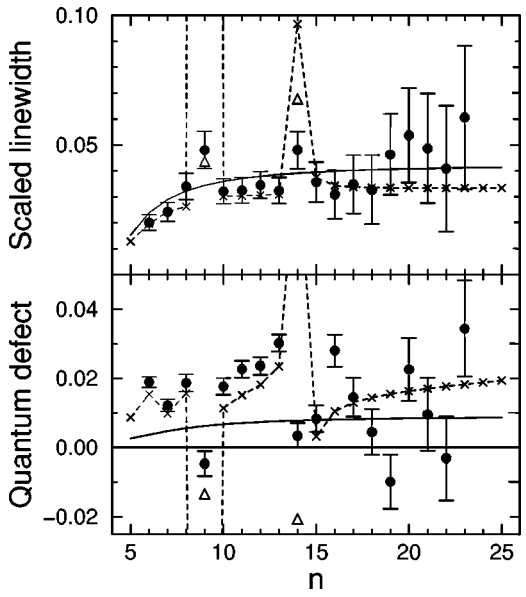

FIG. 6. Quantum defects and scaled autoionization linewidths of the $6p_{1/2}ng[k=9/2]$ states of barium. The solid line for the width may be fitted to $0.0426-0.671/n^2$. See Fig. 1 for details.

tudes in our previous treatment [11]. In fact, one can check here that second-order contributions to the fine-structure autoionization width affect only this partial probability by about 10% and the total autoionization width by 3%, since the fine-structure transition contributes here for only 30%, as a rule, of the total width if n is larger than 8. Finally, one notices again several unexplained oscillations in the quantum defects, for instance if $n=17$, 20, or 24. This emphasizes the need for more accurate measurements in this large-n region.

The $6p_{3/2}ng[k=11/2]$ quantum defects and widths appear in Fig. 4. The scaled linewidths are again well reproduced, except for fluctuations around $n=11$ or 17, which seem to be experiment artifacts. Here the fine-structure transitions contribute, if $n>8$, to the linewidth for less than 2%. As mentioned above concerning the $6p_{3/2}6g[11/2]$ level, the computed quantum defects lie systematically below the measured ones by roughly 0.01 units, i.e., several times the error bars. Interestingly, one will notice that, accounting for the quadrupolar interaction $6p_{3/2}ng-6p_{1/2}\nu i$ at second order, the disagreement is reduced by a factor of 2. Therefore, to improve the computation one might include quadrupoles at second order, but consistency would require considering equally dipole-dipole-quadrupole terms at third order, as well as fourth-order contributions containing the product of four dipoles. Such computation is lengthy though tractable *a priori*, and has not been attempted here.

Finally, we will briefly discuss the $6p_{1/2}ng$ case illustrated by Figs. 5 and 6. We did not try to compare our results to those of Jones and Gallagher [7] because this work does not specify the k value. In the $k=7/2$ case, no experimental data are available other than those discussed in Tables III and IV. Setting aside the above discussed $n=9$ and 14 states, the $k=9/2$ computed linewidths agree with measurements, even without quadrupoles at second order. Conversely, one notices that inclusion of the quadrupolar interaction $6p_{1/2}ng-6p_{3/2}\nu g$ at second order improves the theory-experiment computed agreement on quantum defects. Lastly, the rapid variation of the experimental quantum defects in the $n=16-23$ region, where no perturber is expected, emphasizes again the need for more accurate measurements.

B. $6p_jnh$ states

The even-parity $6p_jnh[J=4,5,6]$ states of barium have been analyzed in some detail by Bente and Hogervorst [33]. As mentioned in the beginning of this section, the data from Jones and Gallagher [7] and from Pruvost *et al.* [10] concern energy regions where series interactions are expected to be weak and where usual second-order perturbation theory should apply; here we will not discuss them any further.

The comparison between our predictions and Bente and Hogervorst's measurements [33] is presented in Tables V and VI for the domains of $6p_{1/2}9h-6p_{3/2}6h$ and $6p_{1/2}14h-6p_{3/2}7h$ interaction, respectively. Here we have tried to amend or clarify the assignation of the experimental levels. For instance, four of the $6p_{1/2}9h$ or $6p_{3/2}6h$ levels of Table V appear in their Table 6 with the only label $6p_{1/2}9h$.

The situation here differs somewhat from the $6p_jng$ case previously analyzed. One the one hand, the present level positions agree with experiment. For instance, the $k=9/2$ computed levels in Table V fall inside the experimental error bars using the diagonalization procedure, while plain second-order theory ignoring second-order quadrupolar interaction between the $6p_jnh$ configurations would be less satisfactory. Our $k=11/2$ predictions are only 2 cm^{-1}above the measurements, this discrepancy coming probably from the insufficient number of ''polarizing'' levels as stated above in the $6p_{3/2}ng[11/2]$ case. On the other hand, the experimental widths are systematically greater than the present ones, often by a factor of 2. We are unable to find a reasonable expla-

TABLE V. Position and width of the interacting $6p_{1/2}9h[k]$, $6p_{3/2}6h[k]$ levels in barium. See Table III for details. The experimental data are from Bente and Hogervorst Ref. [33]. The zero-order energies are 60 941.69 cm^{-1} and 60 939.08 cm^{-1} for the $6p_{1/2}9h$ and $6p_{3/2}6h$ levels, respectively. The $6p_{3/2}6h[13/2]$ is significantly mixed with the $6p_{1/2}9k[13/2]$, which is included in the diagonalization but not tabulated here.

State	Second order		Diagonalization		Experiment	
$6p_{3/2}6h[7/2]$	60 962.29	1.47	(100%) 60 962.25	1.63		
$6p_{1/2}9h[9/2]$	60 941.29	1.20	(82%) 60 945.56	1.41	60 945.5±0.3	2.8±0.6
$6p_{3/2}6h[9/2]$	60 921.08	1.09	(82%) 60 916.82	0.90	60 916.3±0.3	1.6±0.4
$6p_{1/2}9h[11/2]$	60 941.41	1.27	(94%) 60 943.24	1.37	60 941.1±0.3	3.1±0.6
$6p_{3/2}6h[11/2]$	60 909.48	0.96	(94%) 60 907.66	0.86	60 905.7±0.3	1.1±0.4
$6p_{3/2}6h[13/2]$	60 950.76	1.27	(76%) 60 957.62	0.97		

nation for that; however, we have no reason to cast serious doubt on the present computation. The simple second-order computation as displayed in Table V does not significantly differ from the diagonalization result and, as stated above, the computation of widths involves here a finite sum over only three ionization thresholds, all of them reachable through dipolar transition. In support of our computation, we notice that in the same Table 6 of Ref. [33] the $6p_{1/2}13h$ width is 2.4 cm^{-1}, while Jones and Gallagher [7] measured 0.51 ± 0.03 cm^{-1}, and in the second-order framework we get 0.52 and 0.56 cm^{-1} for $k=9/2$ and 11/2, respectively.

The situation is more confusing concerning the $6p_{1/2}14h-6p_{3/2}7h$ interaction as shown in Table VI. Tables 6 and 7 of Bente and Hogervorst report not less than 9 distinct states with J between 4 and 6, while only 6 are expected if jk coupling holds. The 61 725.7 cm^{-1} line reported as $6p_{3/2}7h$ could not be assigned here. Comparing to our position predicted at 61 731.6 cm^{-1}, we assume that the 61 733.5 and 61 734.2 cm^{-1} lines labeled as $6p_{1/2}14h$ are both $6p_{1/2}14h[9/2]$; the uncertainty on the positions being 0.3 cm^{-1}, this splitting may be an artifact, it may also correspond to the $J=4-5$ pair separation. Accordingly, we estimate that the 61 736.3 and the 61 737.5 cm^{-1} lines both correspond to our $6p_{1/2}14h[11/2]$ state at 61 738.0 cm^{-1}. The other $6p_{3/2}7h[k]$ states are assigned according to their relative positions; the level at 61 741.0 cm^{-1} in Ref. [33] is assigned as $k=9/2$ instead of 13/2 and we attribute $k=13/2$ instead of 7/2 to the level at 61 756.4 cm^{-1}. As seen in Table VI the overall agreement on positions is acceptable, while the factor of 2 on linewidths is again observed, mainly on the $6p_{3/2}7h$ states. This discussion stresses the need for more accurate measurements on such doubly excited states.

V. DOUBLY EXCITED STATES IN HELIUM AND MULTIPLY CHARGED IONS

Because of the Coulomb degeneracy in the hydrogenic ion spectrum, the above described diagonalization procedure must always be applied when studying doubly excited levels of true two-electron systems such as $2lnl'$ in helium or C^{4+}. Furthermore, while of course a large amount of theoretical data is available for this isoelectronic sequence (see, e.g., Ref. [35]), it mainly concerns rather low L values; data with L larger than 3 are scarce and sometimes unreliable, since large-l orbitals are not systematically included in the computations. Nevertheless, one must mention a recent work on the positronium negative ion [36] using the complex-coordinate rotation method.

A now traditional description that emphasizes the correlated character of the wave function is provided by the doubly excited symmetry basis (DESB) introduced by Wulfman, Herrick, and Sinanoğlu [37]: the DESB states are labeled ${}_n(K,T)^A_N L^\pi$, where N (respectively, n) is the inner (respectively outer) principal quantum number. The (K,T) numbers describe angular correlations, and later Lin [38] introduced the A number that refers to radial correlations. For all the

TABLE VI. Position and width of the interacting $6p_{1/2}14h[k]$, $6p_{3/2}7h[k]$ levels in barium. The zero-order level positions are 61 736.58 and 61 747.80 cm^{-1} for $6p_{1/2}14h$ and $6p_{3/2}7h$, respectively. Experimental data are from Bente and Hogervorst Ref. [33]. Some assignations are new and others amended, as described in the text.

State	Second order		Diagonalization		Experiment	
$6p_{3/2}7h[7/2]$	61 762.36	1.70	(100%) 61 762.35	1.70	61 765.4±0.4	3.7±0.7
$6p_{1/2}14h[9/2]$	61 736.47	0.43	(64%) 61 731.62	0.57	61 733.5±0.3	0.7±0.4
					61 734.2±0.3	0.7±0.4
$6p_{3/2}7h[9/2]$	61 736.34	1.26	(64%) 61 741.18	1.12	61 741.0±0.3	2.5±0.5
$6p_{1/2}14h[11/2]$	61 736.51	0.46	(77%) 61 738.01	0.76	61 736.3±0.3	1.5±0.4
					61 737.5±0.3	0.7±0.4
$6p_{3/2}7h[11/2]$	61 729.04	1.11	(77%) 61 727.55	0.82	61 730.1±0.3	1.7±0.4
$6p_{3/2}7h[13/2]$	61 755.15	1.51	(98%) 61 755.73	1.47	61 756.4±0.3	1.5±0.4

TABLE VII. Composition of the $3l5l'G$ helium eigenstates in terms of DESB (K,T) quantum numbers. The figures are the squared projections of the present eigenstates over the ${}_n(K,T)_3$ DESB elements, in percent. A sum has been performed for $3 \leqslant n \leqslant 9$. The eigenstate label is given according to the leading configuration, the percentage of which is given in parentheses. For the G^e symmetry, the correlated basis contains six elements, since it also involves the $3pnh$ and $3dni$ series. Accordingly, the G^o DESB includes three elements, since it involves the $3dnh$ series.

	(K,T) character (%)					
Label	(2,0)	(0,0)	$(-2,0)$	(1,1)	$(-1,1)$	(0,2)
$3s5gG^e$ (35.8%)	7.3	40.4	0.8	21.4	29.6	0.6
$3p5fG^e$ (62.8%)	65.7	7.1	0.0	17.9	0.8	8.6
$3d5dG^e$ (97.4%)	23.7	13.9	0.1	45.3	3.7	13.3
$3d5gG^e$ (59.7%)	1.0	17.0	0.1	9.1	1.6	71.2
$3p5gG^o$ (79.0%)				70.7	21.7	7.6
$3d5fG^o$ (79.0%)				27.2	9.6	63.2

large-L states considered here, the A value is zero as there is no significant overlap between the wave function of both electrons. Since we only consider here light elements, the spin-orbit effect is ignored for both electrons, and because exchange is expected to be very small for large-l states, we also drop the total spin S when labeling them. However, even at this early stage we must mention the probable inadequacy of DESB quantum numbers for such large-L states. First, in the DESB elements both electrons have definite principal quantum numbers N and n, and experience the same nucleus charge, e.g., $Z=2$ for helium. A more appropriate choice would be to attribute a screened nucleus charge $Z-1$ to the outer electron and to allow a superposition of n values; however, Lin and Macek [39] have checked that usually such a procedure hardly improves the wave function quality. Even more, these authors, considering the $n(-1,0)_2^0\ {}^1P^o$ states in helium, labeled $2pnd\,{}^1P^o$ in the independent-particle picture, demonstrated that such $A=0$ states are poorly described within the DESB framework. The present paper addresses the question of $A=0$ states with higher L values.

A. $Nlnl'$ series of helium

As a typical result of the present diagonalization method, we give in Table VII for each of the $3l5l'G^e$ eigenstates, the squared projections over the ${}_n(K,T)_3$ DESB states with n summed from 3 to 9. It was checked that higher n values contribute for less than 10^{-4} to the eigenstate normalization. As mentioned above, in our formalism, the zero-order Hamiltonian assumes full screening, i.e., in a ''configuration'' like $3d5g$ the $3d$ orbital corresponds to a Coulomb charge $Z=2$, while the $5g$ orbital corresponds to a screened charge $\zeta=Z-1$. Thus, in evaluating the projection of the kth eigenstate of total angular orbital momentum L and parity π,

$$|\Psi_k\rangle=\sum_i c_{ik}|(Z=2)3l_i(\zeta=1)5\lambda_i\rangle, \tag{5.1}$$

over the ${}_n(K,T)_3$ state, we must evaluate the sum

$$\langle {}_n(K,T)_3L^\pi|\Psi_k\rangle=\sum_{ij} c_{ik}\delta_{l_il_j}\delta_{\lambda_i\lambda_j}\langle {}_n(K,T)_3L^\pi|3l_jn\lambda_j\rangle \times\langle(Z=2)n\lambda_j|(\zeta=1)5\lambda_i\rangle. \tag{5.2}$$

On the right-hand side of Eq. (5.2), the second and third factors account for the orthogonality of the inner- and outer-electron angular parts, the fourth factor is proportional to the well known $9j$ coefficient [37] involving (K,T), and the last one is an overlap integral of hydrogenic functions of the same l but different Z. These integrals have been simply computed using the analytical expressions of the wave functions. The main DESB n values that have a significant projection on the present eigenstates range from 5 to 7. Examination of Table VII reveals that some of the presently computed eigenstates are reasonably characterized by the DESB numbers, such as the second eigenstate labeled as ''$3p5fG^e$,'' for which the squared projection on the $(K,T)=(2,0)$ levels is about 66%. Conversely, it appears that, for many of them, the (K,T) description is a rough approximation; for instance, the first eigenstate in this table, labeled ''$3s5gG^e$,'' bears only 40% of (2,0) character and almost 30% of $(-1,1)$ character.

Nevertheless, the $3l5l'$ states in helium do not provide a fully quantitative test for the present formalism, since the overlap of both electron orbitals is significant except for the largest L values (5 or 6) for which comparison data is lacking; for instance, the $3p$ classical orbital extends up to 8.5 a.u. from the nucleus, while the $5f$ classical inner turning point is at 7 Bohr radii. Therefore, we present in Table VIII the newly derived quantum defects and autoionization linewidths for $3l7l'L \geqslant 5$. Configuration mixing is still very significant for H states: for instance, the state labeled $3s7h$ contains only 42% of this character and a strong admixture of $3d7h$ and $3p7g$. Among the displayed eigenstates in the list, only the $3d7fH^o$ is probably not very accurate, since the $3d$ classical outer turning point is 7.10 while the $7f$ inner turning point is 6.42; besides, the second-order shift of this eigenstate involves a significant contribution from the $4f\nu d$ series, for which the nonoverlap hypothesis clearly breaks down. However, the mixing of this eigenstate with the four other H^o states is very weak (2%), so we believe the four other eigenstates to be correctly predicted; and while its quantum defect (0.459) is probably inaccurate (subtracting the $4f\nu d$ contribution, it changes to 0.259), its linewidth is certainly reasonable because it mostly involves the transition to the $2p\epsilon g$ continuum, well described in the long-range framework—this behavior is also corroborated by the C^{4+} analysis below. Though other theoretical data are missing, one may notice that a large-l state such as $3d7hK^o$ may have a non-negligible quantum defect (0.134) which we believe to be accurately predicted here, since second-order perturbation mainly involves perturbation by the $3p\nu i$ series, well described within the present long-range formalism. Comparing the data in Table VIII to typical $6p_jnl$ data in barium, it appears that while for a given l the quantum defects have the same order of magnitude, the linewidths are much less in helium, usually well below 1 cm^{-1}. This arises from the fact

TABLE VIII. Doubly excited $3l7l'$ states in helium for $L \geqslant 5$. Autoionization widths are in atomic units. The notation $a(-b)$ stands for $a \times 10^{-b}$. Only configurations contributing for at least 10% are mentioned.

Label	Leading configuration	Other configurations	Quantum defect	Width
H^o	$3s7h$ (42%)	$3d7h$ (29%), $3p7g$ (27%)	−0.026 70	6.05(−7)
	$3p7g$ (70%)	$3s7h$ (19%)	0.049 54	1.00(−6)
	$3p7i$ (99%)		−0.095 375	2.93(−10)
	$3d7f$ (98%)		0.459 01[a]	3.69(−5)
	$3d7h$ (61%)	$3s7h$ (38%)	0.090 08	3.03(−9)
H^e	$3p7h$ (68%)	$3d7g$ (32%)	0.116 21[b]	2.89(−7)
	$3d7g$ (68%)	$3p7h$ (32%)	0.130 76[c]	6.06(−7)
	$3d7i$ (100%)		−0.076 76	4.49(−12)
I^e	$3s7i$ (52%)	$3d7i$ (33%), $3p7h$ (14%)	−0.031 61	9.85(−9)
	$3p7h$ (84%)	$3s7i$ (10%)	0.041 33	3.95(−8)
	$3d7g$ (99%)		0.211 67[d]	2.21(−6)
	$3d7i$ (62%)	$3s7i$ (38%)	0.053 39	3.07(−11)
I^o	$3p7i$ (95%)		0.053 63	1.32(−9)
	$3d7h$ (95%)		0.089 74	2.59(−8)
K^o	$3p7i$ (100%)		0.038 78	5.74(−10)
	$3d7h$ (100%)		0.134 47	6.49(−8)
K^e	$3d7i$ (100%)		0.061 40	3.20(−10)
L^e	$3d7i$ (100%)		0.096 08	7.45(−10)

[a]0.2585 if the $4f\nu d$ contribution is removed.
[b]0.1091 if the $4f\nu f$ contribution is removed.
[c]0.1159 if the $4f\nu f$ contribution is removed.
[d]0.1695 if the $4f\nu f$ contribution is removed.

that in helium, the autoionization occurs toward the $1s$ or $2l$ threshold with a large electron energy, which disfavors such a process.

B. $Nlnl'$ series in C^{4+}

Bachau *et al.* [35] have published a large amount of data about the $3lnl'$ states with $n \leqslant 5$ in helium and multiply charged states with $Z \leqslant 10$. In order to interpret charge exchange experiment, van der Hart and Hansen [40] have carefully analyzed the singlet states $2lnl'$ in doubly excited heliumlike carbon with $n \leqslant 7$ and $3lnl'$ with $n \leqslant 5$. As detailed in Sec. II, the present formalism requires that the inner- and outer-electron wave functions not overlap; while the $2l5l'$ or states with $l' > 2$ fulfills this requirement, it is hardly the case for most of the $3l5l'$ states considered below: for instance, the inner $3s$ electron has a classical outer turning point at $r = 3$ Bohr radii while an outer $5f$ electron has a classical inner turning point at $r = 1.39$. However, in order to assess the validity of our large-l treatment, some data will be given for a total L increasing from 4 to 6.

In Table IX we compare our $2lnl$ results with $n = 5$ and 7 and $L > 2$ with the *B*-spline predictions of van der Hart and Hansen. At second order the $Nl\nu l'$ perturbing series with N up to 10 and l up to 3 have been included, which correspond to 34 valence states and therefore several tens of perturbing series. Though our computations were made using the previously described diagonalization procedure with second-order correction, one must mention that in the present framework the interaction matrix at first order turns out to be purely diagonal; due to the long-range approximation leading to susbtitute, e.g., $\langle 2s|r|2p\rangle\langle 5f|r^{-2}|5g\rangle$ to $\langle 2s5f|r_</r_>{}^2|2p5g\rangle$, the outer-electron contribution is canceled because of the Pasternack-Sternheimer identity [41]. The situation is different for the $3l5l'$ states in which, for instance, the $\langle 3s|r^2|3d\rangle\langle 5g|r^{-3}|5g\rangle$ nondiagonal element does not vanish. Another peculiarity of the $2lnl'$ states is that some of them are metastable versus autoionization. For instance the $2p5fF$ cannot decay towards a $1s\epsilon l$ state because of angular momentum conservation. Besides, a state like $2s5gG$, which in our theoretical framework does not interact with $2p5f$, will also be stable versus autoionization; however, going beyond the long-range approximation where the Pasternack-Sternheimer identity cancels the matrix element, the $\langle 2s5g|r_</r_>^2|2p5f\rangle$ differs from 0 and this small configuration mixing gives a nonzero autoionization probability to this eigenstate; nevertheless looking at van der Hart and Hansen's data in Table IX one realizes that this results in very small autoionization probabilities. Considering the set of quantum defects and the linewidths reported in this table, one notices a fair agreement between both computations. Amazingly enough, the $2p5dF$ and $2p7dF$ linewidths are accurately predicted within the present formalism, though the large-l hypothesis does not apply. Conversely, their quantum defects are not accurately obtained within the present formalism, because second-order correction involves interaction with the $Nd\nu p$ series (N values from 3 to 10 are included here). By simply ignoring these interactions, one

TABLE IX. Quantum defects and autoionization widths of $2lnl'$ states in C^{4+}. Widths are in atomic units. The *B*-spline computation by van der Hart and Hansen Ref. [40] concerns singlet states. The notation $a(-b)$ stands for $a\times10^{-b}$.

L^π label	Leading configuration	Quantum defect		Autoionization width	
		B-spline	This paper	*B*-spline	This paper
F^o	$2s5f$	0.002 29	0.002 66	9.16(−7)	a
	$2p5g$	−0.013 69	−0.013 65	1.74(−6)	1.09(−9)
	$2p5d$	−0.020 69	−0.292 52[b]	6.47(−5)	6.85(−5)
	$2s7f$	0.002 43	0.003 05	3.34(−7)	a
	$2p7g$	−0.013 82	−0.013 55	4.96(−7)	1.01(−9)
	$2p7d$	−0.017 52	−0.079 64[c]	2.48(−5)	2.69(−5)
F^e	$2p5f$	0.022 98	0.022 84		a
	$2p7f$	0.023 00	0.023 61		a
G^e	$2p5f$	0.004 56	0.006 75	2.92(−6)	3.36(−6)
	$2s5g$	0.000 74	0.000 63	1.83(−7)	a
	$2p7f$	0.005 43	0.007 75[d]	1.37(−6)	1.65(−6)
	$2s7g$	0.000 76	0.000 74	1.43(−7)	a
	$2p7h$	−0.008 37	−0.008 40	6.5(−11)	9.27(−12)
G^o	$2p5g$	0.010 11	0.010 05		a
	$2p7g$	0.010 18	0.010 19		a
H^o	$2p5g$	0.002 54	0.002 81	5.24(−8)	5.66(−8)
	$2p7g$	0.002 33	0.003 05	4.52(−8)	5.10(−8)
	$2s7h$	−0.001 08	0.000 25	1.0(−9)	a
	$2p7i$	−0.005 59	−0.005 28	3.8(−12)	3.65(−14)
H^e	$2p7h$		0.005 38		a
I^e	$2s7i$		0.000 10		a
	$2p7h$		0.001 99		7.70(−10)
I^o	$2p7i$		0.003 18		a
K^o	$2p7i$		0.001 51		4.53(−12)

[a]Metastable (see the text).
[b]If the interaction with $Nd\nu p$ is removed, $\delta=0.001\,12$.
[c]If the interaction with $Nd\nu p$ is removed, $\delta=0.001\,10$.
[d]Includes $Nd\nu d$ contribution; $\delta=0.002\,02$ if removed.

would get quantum defects positive and close to 10^{-3}, in better agreement with the data from Ref. [40]. One may notice in this table the regular decrease of the quantum defects and linewidths with L; some predictions are made for higher l for which data are missing in the literature. As in helium, such large angular momentum data are very scarce.

As a last example, we give in Table X the quantum defects and widths for the $3l5l'$ doubly excited levels of C^{4+}. Within the present formalism, the long-range coupling between the $3l5l'$ does not vanish as it did in the $2lnl'$ case and the present results do include significant configuration mixing at first order. However, the figures in this table must be used with care for two reasons. First, the nonoverlap hypothesis central to the present model is harder to fulfill here; for instance, the $3p$ classical outer turning point is 2.82 a.u. while the $5f$ classical inner turning point is 1.39 a.u. and even the $5g$ orbital has its inner turning point at 2.76 a.u.. Therefore, higher values for the principal quantum number of the outer electron as well as higher values of L would be desirable, unfortunately no reference values are then available. Second, using the zero-order screened energy $-\{(Z/N)^2+[(Z-1)/n]^2\}/2$ as we do here, the $4l3\lambda$ perturbers considered at second order are almost degenerate with the states considered here; however, clearly this degeneracy is an artifact since perturbers such as $4d3d$ or $4f3p$ cannot be described using the present nonoverlap hypothesis. To circumvent this difficulty, we present in Table X both the plain second-order quantum defects (sixth column, value A) and the value obtained after subtracting the contribution of the $4l\nu l'$ series (seventh column, value B). One must note that autoionization processes leave the ion in the $N=1$ or $N=2$ energy level, so this quasiresonance does not affect the widths as they are computed here. In Table X, we compare our model with the *B*-spline method of van der Hart and Hansen [40] and the Feshbach formalism of Bachau *et al.* [35]. The latter work details the singlet and triplet case, which allows to check the importance of exchange effects; they turn out to be moderate for some of the G states but not all of them. The procedure, consisting of subtracting the spurious $4l\nu l'$ as described above, brings our results in significantly better agreement with the other theoretical determinations. The breakdown of nonoverlap hypothesis reasonably explains the residual differences. One also notices that the agreement with other determinations improves with L as ex-

TABLE X. Quantum defects and autoionization widths of $3lnl'$ states in C^{4+}. Widths are in atomic units. Eigenstates are labeled using L^{π} and the dominant configuration. The computation by van der Hart and Hansen Ref. [40] concerns singlet states, while that by Bachau *et al.* Ref. [35] are given for both singlet and triplet states. Two values are given for the quantum defects within the present framework: the first one (*A*) is the plain result including all perturbing series $Nl\nu l'$ with $N \leqslant 10$, $l \leqslant 3$ at second order, while the second one (*B*) excludes some series as detailed in the text and in notes.

Label	Quantum defect					Autoionization width			
	Ref. [40]	Ref. [35]		This paper		Ref. [40]	Ref. [35]		This paper
		$S=0$	$S=1$	(*A*)	(*B*)		$S=0$	$S=1$	
G^e $3d5d$	0.128 74	0.125	0.171	−0.8655	−0.0744[a]	4.044(−3)	4.4(−3)	6.2(−6)	4.62(−3)
$3d5g$	0.062 79	0.064	0.059	0.0033	0.0677[a]	2.256(−4)	3.1(−4)	1.03(−4)	5.73(−6)
$3p5f$	−0.029 36	−0.030	0.092	−0.6292	−0.0128[a]	6.41(−4)	5.9(−4)	2.0(−4)	3.64(−4)
$3s5g$	−0.053 33	−0.055	−0.030	−0.2607	−0.0413[a]	8.87(−4)	1.25(−3)	1.87(−5)	2.29(−4)
G^o $3d5f$	0.128 86	0.130	0.035	1.3432	0.1151[b]	1.09(−4)	8.8(−5)	2.2(−4)	3.76(−4)
$3p5g$	0.059 52	0.059	0.064	−0.4568	0.0605[b]	2.99(−5)	2.4(−5)	3.2(−6)	6.59(−5)
H^o $3p5g$	0.001 70			−0.0397	0.0010[b]	7.50(−5)			6.44(−5)
$3d5f$	−0.045 30			−2.0584	0.0043[b]	1.56(−3)			1.14(−3)
H^e $3d5g$				0.0479					4.27(−5)
I^e $3d5g$				0.0186					1.06(−4)

[a] $4f\nu p, 4d\nu d$ contributions removed.
[b] $4f\nu d$ contribution removed.

pected. We derive here new values for H^e and I^e levels. Finally, let us mention that the present formalism is fully adapted to determine positions and widths of states with more dissymetric excitation and larger L such as, e.g., $3l10l'H$.

VI. CONCLUSION

Using a new theoretical framework based on diagonalization of the long-range form of the electronic interaction plus second-order correction, we have been able to make accurate predictions about the position and width of a series of strongly interacting levels in large-l alkaline-earth atoms. Some new or amended assignations have been made for previously reported levels. In barium, the $6p_jng$ experimental level positions and widths have been accurately reproduced. More significant discrepancy remains on the $6p_jnh$ levels for which additional experimental data would be of great value. In helium, one has checked that though configuration mixing is important, the collective quantum numbers (K,T) are only partially relevant. When the overlap between both electron wave functions is weak, the present formalism fairly well agrees with more complex ones such as *B* splines or Feshbach theory. Finally, let us mention that autoionization probability has been considered here only through the first-order Fermi Golden Rule. When one has to consider interacting series such as $5d_{3/2}ng$ and $5d_{5/2}ng$ in barium, the computation of autoionization linewidths including the polarization effect by, e.g., $6p_{3/2}nf,h$ series must involve the second-order Fermi Golden Rule. The present formalism is quite suitable for dealing with such effects.

ACKNOWLEDGMENTS

The author wishes to express his gratitude to Professor E. de Prunelé for helpul advice and to Dr. J. Pascale for a careful reading of the manuscript.

[1] M. Aymar, C.H. Greene, and E. Luc-Koenig, Rev. Mod. Phys. **68**, 1015 (1996).
[2] U. Fano, Rep. Prog. Phys. **46**, 97 (1983); C.D. Lin, Phys. Rep. **257**, 1 (1995); G. Tanner, K. Richter, and J.-M. Rost, Rev. Mod. Phys. **72**, 497 (2000).
[3] W. Sandner, Comments At. Mol. Phys. **20**, 171 (1987); W. Hogervorst, *ibid.* **29**, 245 (1993).
[4] L. Meng, C.O. Reinhold, and R.E. Olson, Phys. Rev. A **42**, 5286 (1990); A.K. Kazansky, J. Phys. B **25**, L381 (1992); S. Martin, J. Bernard, L. Chen, A. Denis, and J. Désesquelles, Phys. Rev. A **52**, 1218 (1995); E. Jacquet, M. Chantepie, P. Boduch, C. Laulhé, D. Lecler, and J. Pascale, J. Phys. B **32**, 1151 (1999); C.O. Reinhold, D.G. Arbó, J. Burgdörfer, B. Gervais, E. Lamour, D. Vernhet, and J.P. Rozet, *ibid.* **33**, L111 (2000).
[5] V.L. Jacobs, J. Davis, and P.C. Kepple, Phys. Rev. Lett. **37**, 1350 (1976).
[6] W.E. Cooke and T.F. Gallagher, Phys. Rev. A **19**, 2151 (1979).
[7] R.R. Jones and T.F. Gallagher, Phys. Rev. A **38**, 2846 (1988).
[8] M. Poirier, Phys. Rev. A **38**, 3484 (1988).
[9] T.F. Gallagher, R. Kachru, and N.H. Tran, Phys. Rev. A **26**, 2611 (1982).

[10] L. Pruvost, P. Camus, J.-M. Lecomte, C.R. Mahon, and P. Pillet, J. Phys. B **24**, 4723 (1991).
[11] M. Poirier, Z. Phys. D: At., Mol. Clusters **39**, 189 (1997).
[12] S.M. Jaffe, R. Kachru, H.B. van Linden van den Heuvell, and T.F. Gallagher, Phys. Rev. A **32**, 1480 (1985).
[13] M. Cortés, A. Macías, F. Martín, and A. Riera, J. Phys. B **26**, 3283 (1993).
[14] P.L. Jacobson, D.S. Fisher, C.W. Fehrenbach, W.G. Sturrus, and S.R. Lundeen, Phys. Rev. A **56**, R4361 (1997); **57**, 4065 (1998).
[15] M. Poirier, Z. Phys. D: At., Mol. Clusters **25**, 117 (1993).
[16] M. Poirier, Phys. Rev. A **50**, 1335 (1994).
[17] W.H. Press, S.A. Teukolsky, W.T. Vetterling, and B.P. Flannery, *Numerical Recipes in Fortran* (Cambridge University Press, Cambridge, 1992).
[18] W.R. Johnson, D. Kolb, and K.-N. Huang, At. Data Nucl. Data Tables **28**, 333 (1983).
[19] M. Poirier, J. Phys. B **23**, 4071 (1990).
[20] L.L. Armstrong, Jr., J. Phys. (Paris), Colloq. **C4**, 17 (1970).
[21] M. Poirier and R. Semaoune, J. Phys. B **31**, 1443 (1998).
[22] R.C. Zhao, W. Huang, X.Y. Xu, X.M. Tong, Y.Z. Qu, C.B. Xu, and P. Xue, Phys. Rev. A **53**, 3994 (1996).
[23] A. Maquet, V. Véniard, and T.A. Marian, J. Phys. B **31**, 3743 (1998).
[24] S. Assimopoulos, A. Bolovinos, A. Jimoyiannis, P. Tsekeris, E. Luc-Koenig, and M. Aymar, J. Phys. B **27**, 2471 (1994).
[25] E. Luc-Koenig, A. Bolovinos, M. Aymar, S. Assimopoulos, A. Jimoyiannis, and P. Tsekeris, Z. Phys. D: At., Mol. Clusters **32**, 49 (1994).
[26] S. Assimopoulos, A. Bolovinos, E. Luc-Koenig, S. Cohen, A. Lyras, P. Tsekeris, and M. Aymar, Eur. Phys. J. D **1**, 243 (1998).
[27] C. E. Moore, *Atomic Energy Levels*, Natl. Bur. Stand. U.S. Circ. No 35 (U.S. GPO, Washington, DC, 1971), Vol. 2.
[28] V. Lange, M.A. Khan, U. Eichmann, and W. Sandner, Z. Phys. D: At., Mol. Clusters **18**, 319 (1991).
[29] P. Esherick, Phys. Rev. A **15**, 1920 (1977).
[30] S. Goutis, M. Aymar, M. Kompitsas, and P. Camus, J. Phys. B **25**, 3433 (1992).
[31] A. Jimoyiannis, A. Bolovinos, P. Tsekeris, and P. Camus, Z. Phys. D: At., Mol. Clusters **25**, 135 (1993).
[32] M. Poirier and R. Semaoune, Phys. Rev. A **59**, 3471 (1999).
[33] E.A.J.M. Bente and W. Hogervorst, J. Phys. B **23**, 1403 (1990).
[34] E. Luc-Koenig, M. Aymar, R. van Leeuwen, W. Ubachs, and W. Hogervorst, Phys. Rev. A **52**, 208 (1995).
[35] H. Bachau, F. Martín, A. Riera, and M. Yáñez, At. Data Nucl. Data Tables **48**, 167 (1991).
[36] I. Ivanov and Y.K. Ho, Phys. Rev. A **60**, 1015 (1999).
[37] C. Wulfman, Chem. Phys. Lett. **23**, 370 (1973); D.R. Herrick and O. Sinanoğlu, Phys. Rev. A **11**, 97 (1975); D.R. Herrick, Adv. Chem. Phys. **52**, 1 (1983).
[38] C.D. Lin, Phys. Rev. A **29**, 1019 (1984); Adv. At. Mol. Phys. **22**, 77 (1986).
[39] C.D. Lin and J.H. Macek, Phys. Rev. A **29**, 2317 (1984).
[40] H. van der Hart and J.E. Hansen, J. Phys. B **26**, 641 (1993).
[41] S. Pasternack and R.M. Sternheimer, J. Math. Phys. **3**, 1280 (1962).